Journal of
Applied Sciences

Research Article

A Proposed Adaptive Inverse Multiquadric Shape Parameter Applied with the Dual Reciprocity BEM to Nonlinear and Coupled PDE

[1,3]Sayan Kaennakham and [2]Nissaya Chuathong

[1]School of Mathematics, Institute of Science, Suranaree University of Technology, 30000 Nakhon Ratchasima, Thailand
[2]Faculty of Science, Energy and Environment, King Mongkut's University of Technology North Bangkok (Rayong Campus), 21120 Rayong, Thailand
[3]Center of Excellence in Mathematics, 10400 Bangkok, Thailand

Abstract

Background and Objective: The effect of shape parameter is known to play a crucial role in determining the final results of a collocation-based numerical method. This is also the case for boundary element method where radial basis functions are used to collocate the non-homogeneous term. However, finding an optimal shape parameter is known not to be simple particularly when dealing with complex PDE problems. This investigation was carried out focusing on three purposes. Firstly, it is to propose a new form of shape parameter contained in the inverse-multiquadric RBF that behaves both linearly and exponentially. Secondly, it is to integrate the effect of the local phenomena of the problem at hand into the mechanism of the proposed shape via. the local Reynolds number (Re). Thirdly, the methodology of dual reciprocity boundary element method is studied, applied and computationally implemented to one of the most challenging types of PDEs, 'Burgers equations', famous for its rich in transient, couple and nonlinear phenomena. **Materials and Methods:** The study began with gathering mostly-used and proposed forms of shape parameter and analyzing the general aspects in terms of their affectiveness. A new form of shape parameter that was hoped to alleviate the drawbacks commonly found when using those previously proposed shape parameter. The investigation then moved on applying the methodology of the dual reciprocity boundary element method in conjunction with the newly formulated shape parameter to one of the most challenging forms of PDE namely Burgers' equations. The overall effectiveness of the was evaluated by comparing the results against both their analytical solutions and other numerical works when available in literature. **Results:** Main findings of this work are as follows. Firstly, the method has successfully been applied to Burgers' equations using inverse multiquadric radial basis function at relatively high Reynolds number. Secondly, it is found from all the results obtained in this work that the proposed shape parameter can outperform the fixed ones and certainly deserves further investigation. Lastly, when compared with other numerical works, the accuracy lies in an acceptable level and moreover, gets better when the problem become advective dominated, at high Reynolds number. **Conclusion:** It is found in this work that with its ability to adapt itself locally, the proposed choice of variable shape provides reasonable solutions while requiring only the upper and lower bounding values. This makes choosing the suitable shape much more effective and simpler, particularly when the flow reaches the stage of instability, high Reynolds number.

Competing Interest: The authors have declared that no competing interest exists.

Data Availability: All relevant data are within the paper and its supporting information files.

INTRODUCTION

The radial basis functions (RBFs), φ are commonly found as multivariate functions whose values are dependent only on the distance from the origin and commonly assumed to be strictly positive definite. This means that $\varphi(x) = \varphi(r) \in R$, the set of real numbers, with $x \in R^n$ and $r \in R$ or in other words, on the distance from a point of a given set $\{x_j\}$ and $\varphi(x-x_j) = \varphi(r_j) \in R$ where can normally defined as expressed in Eq. 1:

$$r = \left\| x - x^{\Theta} \right\|_2 = \sqrt{(x_1 - x_1^{\Theta})^2 + \ldots + (x_n - x_n^{\Theta})^2} \qquad (1)$$

for some fixed points $x \in R^n$ and $r_j = \|x-x_j\|_2$ is the Euclidean distance. Two classes of numerical tools that involve the use of RBFs are the so-called 'meshfree method' and 'boundary element method'. There are many forms of RBFs invented, proposed, tested and documented nowadays under the context of finding solution to different type partial differential equations (PDEs). Below is the list of some well-known and most widely used RBFs:

- Linear (LR): $1+r$
- Gaussian (GU): $e^{(-\varepsilon r^2)}$
- Cubic (CU) : r^3
- Polyharmonic (PY) in R^3: r^{2n-1}, $n \in \mathbb{N}$
- Polyharmonic (PY) in R^2: $r^{2n} \ln(r)$, $n \in \mathbb{N}$
- Multiquadric (MQ): $\sqrt{r^2 + \varepsilon^2}$
- Inverse multiquadric (IMQ): $1 / \left[\sqrt{r^2 + \varepsilon^2} \right]$
- Thin-plate spline (TPS): $r^2 \ln(r)$
- Matern/sobolev (MS): $*[K_V (r) r^V]$
- $*[K_V$ is an order Bessel function]

In this study, nevertheless, the RBF type being focused on is the 'Inverse-multiquadric (IMQ)' form expressed as follows:

$$\varphi(r, \varepsilon) = (\varepsilon^2 + r^2)^{\beta} \qquad (2)$$

where, $\beta = \ldots, -3/2, -1/2, 1/2, 3/2, \ldots$ and ε is the so-called 'shape parameter' and is normally given in an '*ad hoc*' manner. Different values of ε, illustrated in Fig. 1, lead to different impact on the final results as well acknowledged. This kind of radial basis function has been proven to be strictly positive definite as nicely documented by Buhmann[1], meaning that the distance matrix of the interpolation problem is invertible. Throughout this study, it focused on the most popular form of the inverse multiquadric, i.e., $\beta = -1/2$, only.
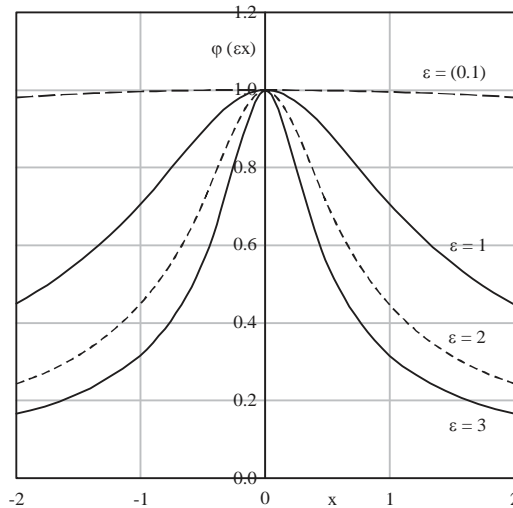
Fig. 1: Infinitely smooth inverse-multiquadric RBF measured numerically at different shape values, ε

Appearing as an alternative numerical method, finite element, finite volume and finite difference, over the last two decades, the boundary element method (BEM) is now known to be another important tool for solving a wide range of applied sciences and engineering that involve linear as well as certain types of nonlinear partial differential equations (PDEs). Like other numerical schemes, the method is not without difficulties or challenges when it faces problems with nonlinear, transient, coupled and nonhomogeneous form of PDEs.

Brebbia and Butterfield[2] proposed an improved version of the scheme and they named it as 'dual reciprocity boundary element method (DRBEM)'. In the process of DRBEM, the solution is divided into two parts: Complementary solutions of its homogeneous form and the particular solutions of the inhomogeneous counterpart. Since the particular solutions are not always available especially in complex problems, the inhomogeneous term of the PDE is approximated by a series of simple functions and transformed to the boundary integrals employing particular solutions of considered problem. The most widely used approximating functions in DRBEM are radial basis functions (RBFs) for which particular solutions can be easily determined[3].

When it comes to using a radial basis function, particularly those forms with the parameter, it is then down to the user's decision to choose what they believe is best and very often this is done under rather '*ad hoc*' manner. For multiquadric (MQ) type of RBF, there are some investigations done on providing information regarding choosing optimal shape value. Hardy[4] suggests that by fixing the shape at

$\varepsilon = 1/(0.815d)$, where, $d = (1/N)\sum_{i=1}^{N} d_i$ and d_i is the distance from the node to its nearest neighbor, good results should be anticipated. Also, in the work of Franke and Schaback[5] where the choice of a fixed shape of the form $\varepsilon = 0.8\sqrt{N}/D$ where, D is the diameter of the smallest circle containing all data nodes, can also be a good alternative.

Some recent attempts to pinpoint the optimal value of ε involve the work of Zhang *et al.*[6] where they demonstrated and concluded that the optimal shape parameter is problem dependent. In 2002, Wang and Lui[7] pointed out that by analyzing the condition number of the collocation matrix, a suitable range of derivable values of ε can be found. Later in 2003, Lee *et al.*[8] suggested that the final numerical solutions obtained are found to be less affected by the method when the approximation is applied locally rather than globally.

At this point, nevertheless, there are several facts to be noticed at. Firstly, most of the proposed forms are concerned with either numerical aspect or fixed values only, meaning that no real physical aspects included or being under consideration. Secondly, all the works were done under the context of pure RBF-collocation methods, nothing is done under DRBEM. Thirdly, the shape parameter contained in the inverse-multiquadric type of RBF has not, by far, been taken a look at. This prompts our initiative idea of this study.

One of the classical non-linear parabolic equation system widely acknowledged as the Burgers' equations, named after the great Physicist[9]. The equations retain the nonlinear of the governing equation in a number of applications, flow through a shock wave traveling in viscous fluid, the phenomena of turbulence, air/water pollution or chemical compound carried by fluids, sedimentation of two kinds of particles in fluid suspensions under the effect of gravity (Burgers[9], Nee and Duan[10]).

For large values of the Reynolds number (Re), one of the major difficulties is due to in-viscid boundary layers produced by the steepening effect of the nonlinear advection term in Burgers' equations. This difficulty is also encountered in an inviscid Navier–Stokes equation for a convection dominated flow and in fact, the famous coupled-Burgers' equations are one of the principle equations used to evaluate any newly proposed numerical methods[11].

This all leads to our main objectives of this investigation which are, firstly, it proposed a new form of shape parameter contained in the inverse-multiquadric RBF. Secondly, the proposed shape was designed to take into consideration the local physical of the problem at hand governed by the dimensionless Reynolds number (Re). Thirdly, the methodology of DRBEM was studied, applied and computationally implemented to one of the most challenging types of PDEs known as 'Burgers' equation', famous for its rich in transient, couple and nonlinear phenomena. The results obtained from this investigation were validated against other alternative numerical works in literature when available.

MATERIALS AND METHODS

DRBEM for Burgers' equations: Let us consider the system of two-dimensional unsteady, nonlinear and coupled Burgers' equations, expressed as follows:

$$\frac{\partial u}{\partial t} + u\frac{\partial u}{\partial x} + v\frac{\partial u}{\partial y} = \frac{1}{Re}\left(\frac{\partial^2 u}{\partial x^2} + \frac{\partial^2 u}{\partial y^2}\right) \quad (3)$$

$$\frac{\partial v}{\partial t} + u\frac{\partial v}{\partial x} + v\frac{\partial v}{\partial y} = \frac{1}{Re}\left(\frac{\partial^2 v}{\partial x^2} + \frac{\partial^2 v}{\partial y^2}\right) \quad (4)$$

Subject to the initial conditions:

$$u(x, y, 0) = \beta_1(x, y) \text{ and } v(x, y, 0) = \beta_2(x, y)$$

and the boundary conditions:

$$u(x, y, t) = \gamma_1(x, y, t) \text{ and } v(x, y, t) = \gamma_2(x, y, t)$$

for $(x, y) \in \partial\Omega$, t>0, u(x, y, t) and v(x, y, t) are the velocity components, β_1, β_2, γ_1 and γ_2 are known functions and Re is the Reynolds number, described by Keannakham *et al.*[12].

The mathematical construction of the dual reciprocity boundary element method can start with the Poisson equation as follows:

$$\nabla^2 u = b(x, y) \quad (5)$$

Which as its equivalent integral form, given by Brebbia and Butterfield[2] as:

$$c_i u_i + \int_\Gamma q^* u d\Gamma - \int_\Gamma u^* q d\Gamma = \sum_{j=1}^{N+L} \alpha_j \left(c_i \hat{u}_{ij} + \int_\Gamma q^* \hat{u}_j d\Gamma - \int_\Gamma u^* \hat{q}_j d\Gamma \right) \quad (6)$$

where, u* the fundamental solution and the term is defined as $\hat{q}_j = \dfrac{\partial \hat{u}_j}{\partial n}$, where n is the unit outward normal to Γ and can be written as follows:

$$\hat{q}_j = \frac{\partial \hat{u}_j}{\partial x}\frac{\partial x}{\partial n} + \frac{\partial \hat{u}_j}{\partial y}\frac{\partial y}{\partial n} \quad (7)$$

Next, the method was applied with N and L being the number of boundary and internal nodes, respectively, b can be now approximated by:

$$b_i(x, y) \approx \sum_{j=1}^{N+L} \alpha_j f_{ij}(x, y)$$

Or, can be written as follows:

$$b = F\alpha \tag{8}$$

Or:

$$\begin{bmatrix} b_1(x,y) \\ b_2(x,y) \\ b_3(x,y) \\ \vdots \\ b_{N+L}(x,y) \end{bmatrix} = \begin{bmatrix} f_{11}(x,y) & \cdots & f_{1(N+L)}(x,y) \\ f_{21}(x,y) & \cdots & f_{2(N+L)}(x,y) \\ \vdots & \vdots & \vdots \\ f_{(N+L)1}(x,y) & \cdots & f_{(N+L)(N+L)}(x,y) \end{bmatrix} \begin{bmatrix} \alpha_1 \\ \alpha_2 \\ \alpha_3 \\ \vdots \\ \alpha_{N+L} \end{bmatrix}$$

where, the function f is the radial basis function which is, in this work, the inverse-multiquadric type. With this radial basis function, then the following form was obtained:

$$\nabla^2 \hat{u}_j = f_j \tag{9}$$

for some particular solution, $\hat{u}_j$. Applying Green's theorem, the boundary element approximation to Eq. 9, then it becomes, at a node ith:

$$c_i u_i + \sum_{k=1}^{N} \int_{\Gamma_k} q^* u d\Gamma - \sum_{k=1}^{N} \int_{\Gamma_k} u^* q d\Gamma$$
$$= \sum_{j=1}^{N+L} \alpha_j \left(c_i \hat{u}_{ij} + \sum_{k=1}^{N} \int_{\Gamma_k} q^* \hat{u}_j d\Gamma - \sum_{k=1}^{N} \int_{\Gamma_k} u^* \hat{q}_j d\Gamma \right) \tag{10}$$

For i = 1, 2,..., N.

After introducing the interpolation function and integrating over each boundary elements, the above Eq. 10 can be re-written in terms of nodal values as:

$$c_i u_i + \sum_{k=1}^{N} H_{ik} u_k - \sum_{k=1}^{N} G_{ik} q_k$$
$$= \sum_{j=1}^{N+L} \alpha_j \left(c_i \hat{u}_{ij} + \sum_{k=1}^{N} H_{ik} \hat{u}_{kj} - \sum_{k=1}^{N} G_{ik} \hat{q}_{kj} \right) \tag{11}$$

where, the definition of the terms H_{ik} and G_{ik} are described by Toutip[13]. The index k is used for the boundary nodes which are

the field points. After application to all boundary nodes, using a collocation technique, Eq. 11 can be compactly expressed in matrix form as follows:

$$Hu - Gq = (H\hat{U} - G\hat{Q})\alpha \tag{12}$$

By substituting $\alpha = F^{-1}b$ from Eq. 8, into Eq. 12 making the right hand side of Eq. 12 a known vector. Therefore, it can be rewritten as:

$$Hu\text{-}Gq = d \tag{13}$$

where, $d = (H\hat{U} - G\hat{Q})F^{-1}b$. Applying boundary conditions to Eq. 13, then it can be seen as the simple form as follows:

$$Ax = y \tag{14}$$

where, x contains N unknown boundary values of u's and q's.

After Eq. 14 is solved using standard techniques such as Gaussian elimination, the values at any internal node can be calculated from Eq. 11, i.e., $c_i = 1$ as expressed in Eq. 15 where each one involving a separate multiplication of known vectors and matrices:

$$u_i = -\sum_{k=1}^{N} H_{ik} u_k + \sum_{k=1}^{N} G_{ik} q_k$$
$$= \sum_{j=1}^{N+L} \alpha_j \left(c_i \hat{u}_{ij} + \sum_{k=1}^{N} H_{ik} \hat{u}_{kj} - \sum_{k=1}^{N} G_{ik} \hat{q}_{kj} \right) \tag{15}$$

Firstly, substituting Eq. 12 into Eq. 11 to get the equation system matrix which expressed as:

$$Hu - Gq = (H\hat{U} - G\hat{Q})F^{-1}b \tag{16}$$

It is then possible to approximate the terms, $u\dfrac{\partial u}{\partial x}$, $u\dfrac{\partial u}{\partial y}$, $v\dfrac{\partial u}{\partial x}$ and $v\dfrac{\partial u}{\partial y}$ as below:

$$u\frac{\partial u}{\partial x} = U\frac{\partial F}{\partial x}F^{-1}u, \ u\frac{\partial v}{\partial x} = U\frac{\partial F}{\partial x}F^{-1}v$$
$$v\frac{\partial u}{\partial y} = V\frac{\partial F}{\partial y}F^{-1}v, \ v\frac{\partial u}{\partial y} = V\frac{\partial F}{\partial y}F^{-1}u \tag{17}$$

From Eq. 16 and Eq. 17, the following was obtained:

$$Hu - Gq = (H\hat{U} - G\hat{Q})F^{-1}b_i \tag{18}$$

and:

$$Hv - Gz = \left(H\hat{V} - G\hat{Z}\right)F^{-1}b_2 \qquad (19)$$

where, $q = \dfrac{\partial u}{\partial n}, \quad z = \dfrac{\partial v}{\partial n}$ and:

$$b_1 = Re\left(\frac{\partial u}{\partial t} + u\frac{\partial u}{\partial x} + v\frac{\partial u}{\partial y}\right) \qquad (20)$$

and

$$b_2 = Re\left(\frac{\partial v}{\partial t} + u\frac{\partial v}{\partial x} + v\frac{\partial v}{\partial y}\right) \qquad (21)$$

In the case, if $\hat{U}$, $\hat{V}$ were considered to be generated by using the same redial basis function, then:

$$\hat{U} = \hat{V} \text{ and } \hat{Q} = \hat{Z} \qquad (22)$$

For the time derivatives, the forward difference method was used to approximate time derivative $\dot{u} = \dfrac{u^{t+1} - u^t}{\Delta t}$ and $\dot{v} = \dfrac{v^{t+1} - v^t}{\Delta t}$. Now, substituting Eq. 32-35, 38 and 39 in Eq. 43 and 44, then the following was obtained:

$$(Hu - Gq) = ARe\left(\dot{u} + U\frac{\partial F}{\partial x}F^{-1}u + V\frac{\partial F}{\partial y}F^{-1}u\right) \qquad (23)$$

and:

$$(Hv - Gz) = ARe\left(\dot{v} + U\frac{\partial F}{\partial x}F^{-1}v + V\frac{\partial F}{\partial y}F^{-1}v\right) \qquad (24)$$

by setting $A = \left(H\hat{U} - G\hat{Q}\right)F^{-1}$ and $C = U\dfrac{\partial F}{\partial x}F^{-1} + V\dfrac{\partial F}{\partial x}F^{-1}$ then the final forms of DRBEM for this type of equations $A = \pi r^2$ as follows:

$$\left(\left(Re\right)AC + \frac{SRe}{\Delta t} - H\right)u^{t+1} + Gq^{t+1} = \frac{ReS}{\Delta t}u^t \qquad (25)$$

and:

$$\left(\left(Re\right)AC + \frac{SRe}{\Delta t} - H\right)v^{t+1} + Gz^{t+1} = \frac{ReS}{\Delta t}v^t \qquad (26)$$

Note that the elements of matrices H, G and A depend only on geometrical data. Thus, they can all be computed once and stored.

Table 1: Some choices proposed in literature

References	Formulation of ε for j^{th}-element
Kansa[14]	$\varepsilon_j = \left[\varepsilon_{min}^2\left(\dfrac{\varepsilon_{max}^2}{\varepsilon_{min}^2}\right)^{\frac{j-1}{N-1}}\right]^{\frac{1}{2}}$, with $j = 1, 2,..., N$
Kansa and Carlson[15]	$\varepsilon_j = \varepsilon_{min} + \left(\dfrac{\varepsilon_{max} - \varepsilon_{min}}{N-1}\right)j$ with $j = 0, 1, 2,..., N\text{-}1$
Sarra[16]	$\varepsilon_j = \varepsilon_{min} + (\varepsilon_{max}\text{-}\varepsilon_{min}) \times r$ and $(1, N)$
Sarra and Sturgill[17]	$\varepsilon_j = \dfrac{\mu}{h_n}\left[\varepsilon_{min} + \Xi \times r \text{ and}(1, N)\right]$ with $\Xi = (\varepsilon_{max}\text{-}\varepsilon_{min})$

Proposed variable IMQ shape: Regarding the studies in the search for optimal choice of the shape parameter, many outstanding and well-known forms proposed in the past are listed in Table 1. In this table, it can be seen that one of the first attempts in searching for variable form of shape parameter was done in 1990 by Kansa[14] which the experimental manner was looked at. This form was then modified by Kansa and Carlson[15]. In their work, ε_{min}^2 and ε_{min}^2 were observed that the better quality of results can be achieved if these two values vary by several orders of magnitude. Sarra[16] and Sarra and Sturgill[17] later invented a linear form of variable shape parameter and applied to both interpolation and some benchmark partial differential equations. The command 'rand' is the MATLAB function that returns uniformly distributed pseudo-random numbers on the unit interval. In their study, the variable form of shape parameter was shown to be superior to the fixed form particularly when the system includes some information about the minimum distance of a center to its nearest neighbor h_n, with also a user input value μ. It is, nevertheless, to be noticed that all the attempts mentioned so far are under the context of the collocation meshfree method where there is no, by far, work carried out under the DRBEM. This leads to one of our main objectives of this investigation.

In this study, it proposed a new form of variable shape parameter where both linear and exponential manners are taken into consideration, expressed as in Eq. 27-30:

$$\varepsilon_j = \zeta \cdot \varepsilon_{exp} + (1\text{-}\zeta) \cdot \varepsilon_{lin} \qquad (27)$$

Where:

$$\varepsilon_{exp} = \left[\varepsilon_{min}^2\left(\frac{\varepsilon_{max}^2}{\varepsilon_{min}^2}\right)^{\zeta}\right]^{\frac{1}{2}} \qquad (28)$$

and:

$$\varepsilon_{lin} = [\varepsilon_{min} + (\varepsilon_{max}\text{-}\varepsilon_{min})] \qquad (29)$$

and ζ is set to correspond to local Reynolds number (Re_{ij}) and is defined as follows:

$$\zeta = \frac{Re_{ij}}{\max\limits_{i \neq j}\left|Re_{ij}\right|} \tag{30}$$

and the dimensionless number called The Reynolds Number, (Re), which is the ratio of the inertia to the viscous or friction force and is defined, in a global sense, as:

$$Re_{Global} = \frac{UL}{\nu} \tag{31}$$

where, L is the characteristic length scale, U is the velocity and v is the kinematic viscosity. In this investigation, this number is locally defined as:

$$\begin{aligned} Re_{ij}^{t} &= \frac{U_i^t L_{ij}}{\nu^t} \\ &= \frac{\left|\sqrt{(u_i^t)^2 + (v_i^t)^2}\right| \cdot \left\|x_i - x_j\right\|_2}{\nu^t} \end{aligned} \tag{32}$$

where, ν^t is defined in a local sense as:

$$\nu^t = \frac{1}{Re_{Global}}\left[\frac{1}{N+L}\sum_{i=1}^{N+L}\sqrt{(u_i^{t-1})^2 + (v_i^{t-1})^2}\right] \tag{33}$$

where, N+L is the total number of nodes (both boundary and internal) involved in the system, the superscript t indicates the time level. The subscript i and j mean at ith and jth node, respectively.

Numerical setup: The computation process is done following the below algorithm:

• Initializing the matrix C by setting it to zero for both U and V
• Setting all the values appearing in Eq. 25 and 26 and then applying the initial conditions to the right hand side and boundary condition to the left hand side, reducing to the form Ax = y
• Using the iterative scheme as $A^{(k)}x^{(k)} = y^{(k)}$, where, k = 1, 2, 3.... The solutions of for both U and Vcan then be achieved when the algorithm stops i.e. when it reaches the following condition:

$$\max\limits_{i}\left|x_i^{(k+1)} - x_i^{(k1)}\right| < \omega \tag{34}$$

with an user's given value of a tolerance ω.

• The solutions obtained from step 3 will be used as the initial conditions in next time-step and the computing process continues until the time level given is reached

All numerical simulations under this investigation were carried out on an Intel(R) Core(TM) i7-5500U CPU @ 2.4 GHz with 8.00 GB of RAM.

RESULTS

To demonstrate the effectiveness of the proposed shape parameter, the methodology was applied to two benchmark examples governed by the Burgers' form of equations. The results obtained were validated against both the corresponding exact solutions and those published in literature. In some cases, the root mean square (RMS) error norm was used and it was defined as below:

$$RMS = \sqrt{\frac{\sum\limits_{i=1}^{N+L}\left(u_i^{exact} - u_i^{num}\right)^2}{N+L}} \tag{35}$$

It was noted here that the Reynolds number written as 'Re' from now on is the global Reynolds number described and used in Eq. 31-33.

Experiment 1: The first example was the well-known form where its exact solutions for validation were provided by using a Hopf-Cole transformation nicely done by Fletcher[18] and was expressed as follows:

$$u(x,\ y,\ t) = \frac{3}{4} - \frac{1}{4}\left[1 + \Phi\right]^{-1} \tag{36}$$

and:

$$v(x,\ y,\ t) = \frac{3}{4} + \frac{1}{4}\left[1 + \Phi\right]^{-1} \tag{37}$$

where, $\Phi = \exp\left((-4x + 4y - t)\dfrac{Re}{32}\right)$ and both the initial and boundary conditions to be imposed to the equation system was generated directly from the above exact form over the domain $\Omega = \{(x, y): 0 \leq x \leq 1,\ 0 \leq y \leq 1\}$.

Table 2-9 showed the computed values of both U- and V-values for Re = 1 at t = 0.01 and Re = 10 at t = 0.5, respectively, obtained from this work compared against both its' exact solutions and those provided by Biazar and Aminikhah[19]. In this case, only 13 internal nodes were chosen and it can be seen that the method constructed in this study performed well and results agreed nicely with both references.

Table 2: Comparison of U-velocity for Re = 1, t = 0.01 with boundary node N = 80 and internal nodes L = 13, for $(\varepsilon_{min}, \varepsilon_{max}) = (0.1, 1)$

| | $(\varepsilon_{min}, \varepsilon_{max}) = (0.1, 1)$ | | | |
Points	Exact	Numerical	Fixed $\varepsilon = 3$	Biazar and Aminikhah[19]
(0.1, 0.1)	0.62498047	0.62497105	0.62801251	0.62498046
(0.5, 0.1)	0.62185613	0.62182512	0.64215822	0.62185614
(0.9, 0.1)	0.61873572	0.61872154	0.62501143	0.61873572
(0.3, 0.3)	0.62498047	0.62496988	0.63265822	0.62498046
(0.7, 0.3)	0.62185613	0.62172788	0.63220140	0.62185614
(0.1, 0.5)	0.62810483	0.62804458	0.64011253	0.62810483
(0.5, 0.5)	0.62498047	0.62496250	0.61254870	0.62498046
(0.9, 0.5)	0.62185613	0.62185688	0.63251115	0.62185614

Table 3: Comparison of U-velocity for Re = 1, t = 0.01 with boundary nodes N = 80 and internal nodes L = 13, for $(\varepsilon_{min}, \varepsilon_{max}) = (0.1, 10)$

| | $(\varepsilon_{min}, \varepsilon_{max}) = (0.1, 10)$ | | | |
Points	Exact	Numerical	Fixed $\varepsilon = 3$	Biazar and Aminikhah[19]
(0.1, 0.1)	0.624980469	0.624982141	0.625145882	0.624980468
(0.5, 0.1)	0.621856132	0.621852158	0.619528022	0.621856142
(0.9, 0.1)	0.618735721	0.618736528	0.617995862	0.618735722
(0.3, 0.3)	0.624980469	0.624981458	0.623569825	0.624980468
(0.7, 0.3)	0.621856132	0.621852154	0.632541777	0.621856142
(0.1, 0.5)	0.628104832	0.628104589	0.619856722	0.628104835
(0.5, 0.5)	0.624980469	0.624981025	0.612499603	0.624980468
(0.9, 0.5)	0.621856132	0.621853652	0.601548862	0.621856142

Table 4: Comparison of V-velocity for Re = 1, t = 0.01 with boundary nodes N = 80 and internal nodes L = 13, for $(\varepsilon_{min}, \varepsilon_{max}) = (0.1, 1)$

| | $(\varepsilon_{min}, \varepsilon_{max}) = (0.1, 1)$ | | | |
Points	Exact	Numerical	Fixed $\varepsilon = 3$	Biazar and Aminikhah[19]
(0.1, 0.1)	0.87501953	0.87502154	0.86220155	0.87501953
(0.5, 0.1)	0.87814386	0.87810012	0.87201258	0.87814387
(0.9, 0.1)	0.88126427	0.88124585	0.89200258	0.88126428
(0.3, 0.3)	0.87501953	0.87504125	0.85210041	0.87501953
(0.7, 0.3)	0.87814386	0.87813605	0.85236051	0.87814387
(0.1, 0.5)	0.87189517	0.87180128	0.85988622	0.87189517
(0.5, 0.5)	0.87501953	0.87506005	0.86022500	0.87501953
(0.9, 0.5)	0.87814386	0.87811458	0.86002598	0.87814387

Table 5: Comparison of V-velocity for Re = 1, t = 0.01 with boundary nodes N = 80 and internal nodes L = 13, for $(\varepsilon_{min}, \varepsilon_{max}) = (0.1, 10)$

| | $(\varepsilon_{min}, \varepsilon_{max}) = (0.1, 10)$ | | | |
Points	Exact	Numerical	Fixed $\varepsilon = 3$	Biazar and Aminikhah[19]
(0.1, 0.1)	0.875019531	0.875025144	0.882115471	0.875019531
(0.5, 0.1)	0.878143868	0.878141202	0.880258822	0.878143878
(0.9, 0.1)	0.881264279	0.881221110	0.882550144	0.881264281
(0.3, 0.3)	0.875019531	0.875015269	0.890125851	0.875019531
(0.7, 0.3)	0.878143868	0.878142158	0.880114225	0.878143878
(0.1, 0.5)	0.871895173	0.871885962	0.882002569	0.871895177
(0.5, 0.5)	0.875019531	0.875012985	0.892001582	0.875019531
(0.9, 0.5)	0.878143868	0.878125140	0.889958002	0.878143878

Table 6: Comparison of U-velocity for Re = 10, t = 0.5 with boundary nodes N = 80 and internal nodes L = 13 for $(\varepsilon_{min}, \varepsilon_{max}) = (0.1, 1)$

| | $(\varepsilon_{min}, \varepsilon_{max}) = (0.1, 1)$ | | | |
Points	Exact	Numerical	Fixed $\varepsilon = 3$	Biazar and Aminikhah[19]
(0.1, 0.1)	0.61525419	0.61510154	0.62001582	0.615254225
(0.5, 0.1)	0.58539562	0.58444958	0.58002158	0.585395632
(0.9, 0.1)	0.55983733	0.55912958	0.54099852	0.559837332
(0.3, 0.3)	0.61525419	0.61503547	0.60025472	0.615254225
(0.7, 0.3)	0.58539562	0.58283985	0.56988500	0.585395632
(0.1, 0.5)	0.64627528	0.64712698	0.65520225	0.646275273
(0.5, 0.5)	0.61525419	0.61392014	0.60205807	0.615254225
(0.9, 0.5)	0.58539562	0.58412015	0.60221500	0.585395632

Table 7: Comparison of U-velocity for Re = 10, t = 0.5 with boundary nodes N = 80 and internal nodes L = 13, for $(\varepsilon_{min}, \varepsilon_{max}) = (0.1, 10)$

| | $(\varepsilon_{min}, \varepsilon_{max}) = (0.1, 10)$ | | | |
Points	Exact	Numerical	Fixed $\varepsilon = 3$	Biazar and Aminikhah[19]
(0.1, 0.1)	0.6152541	0.61521250	0.62502225	0.615254225
(0.5, 0.1)	0.5853956	0.58493625	0.57988544	0.585395632
(0.9, 0.1)	0.5598373	0.55955520	0.56880220	0.559837332
(0.3, 0.3)	0.6152541	0.61522011	0.60014522	0.615254225
(0.7, 0.3)	0.5853956	0.58430155	0.57015455	0.585395632
(0.1, 0.5)	0.6462752	0.64679210	0.60125884	0.646275273
(0.5, 0.5)	0.6152541	0.61487581	0.60148022	0.615254225
(0.9, 0.5)	0.5853956	0.58478952	0.56990520	0.585395632

Table 8: Comparison of V-values for Re = 10, t = 0.5 with boundary nodes N = 80 and internal nodes L = 13, for $(\varepsilon_{min}, \varepsilon_{max}) = (0.1, 1)$

| | $(\varepsilon_{min}, \varepsilon_{max}) = (0.1, 1)$ | | | |
Points	Exact	Numerical	Fixed $\varepsilon = 3$	Biazar and Aminikhah[19]
(0.1, 0.1)	0.88474580	0.88455261	0.87202582	0.88474577
(0.5, 0.1)	0.91460437	0.91422015	0.90250259	0.91460435
(0.9, 0.1)	0.94016266	0.94012148	0.93695802	0.94016267
(0.3, 0.3)	0.88474580	0.88395820	0.89580024	0.88474577
(0.7, 0.3)	0.91460437	0.91438591	0.90254781	0.91460435
(0.1, 0.5)	0.85372471	0.85246325	0.84255699	0.85372471
(0.5, 0.5)	0.88474580	0.88350225	0.89658025	0.88474577
(0.9, 0.5)	0.91460437	0.91458557	0.90012586	0.91460435

Table 9: Comparison of V-values for Re = 10, t = 0.5 with boundary nodes N = 80 and internal nodes L = 13, for $(\varepsilon_{min}, \varepsilon_{max}) = (0.1, 10)$

| | $(\varepsilon_{min}, \varepsilon_{max}) = (0.1, 10)$ | | | |
Points	Exact	Numerical	Fixed $\varepsilon = 3$	Biazar and Aminikhah[19]
(0.1, 0.1)	0.88474580	0.88448520	0.87589522	0.88474577
(0.5, 0.1)	0.91460437	0.91421025	0.93225862	0.91460435
(0.9, 0.1)	0.94016266	0.94012556	0.93225014	0.94016267
(0.3, 0.3)	0.88474580	0.88321369	0.86922581	0.88474577
(0.7, 0.3)	0.91460437	0.91421140	0.93002581	0.91460435
(0.1, 0.5)	0.85372471	0.85233660	0.86955822	0.85372471
(0.5, 0.5)	0.88474580	0.88347504	0.89002586	0.88474577
(0.9, 0.5)	0.91460437	0.91466905	0.90214552	0.91460435
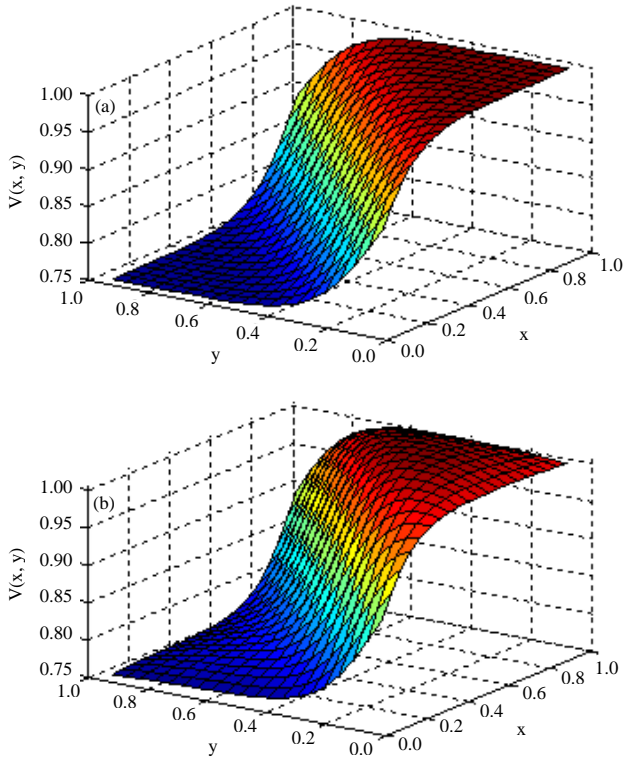
Fig. 2(a-b): Comparison of V-values for $(\varepsilon_{min}, \varepsilon_{max}) = (0.1, 10)$ at $t = 0.1$ with Re = 80 between the exact (left) and the computed ones (right)

Solution profiles of both U- and V-velocity, at moderate Reynolds number, were illustrated in Fig. 2-4 showed the root mean square (RMS) error.

Experiment 2: For this example, it was adopted from the work of Aminikhah[20] for solution validation. This problem is on the domain $\Omega = \{(x, y): 0 \le x \le 1, 0 \le y \le 1\}$ with the following initial and boundary conditions:

$$u(x, y, 0) = -\frac{4\pi \cos(2\pi x)\sin(\pi y)}{Re(2 + \sin(2\pi x)\sin(\pi y))} \quad (38)$$

$$v(x, y, 0) = -\frac{2\pi \sin(2\pi x)\cos(\pi y)}{Re(2 + \sin(2\pi x)\sin(\pi y))} \quad (39)$$

$$u(0, y, t) = u(1, y, t) = u(x, 0, t) \\ = u(x, 1, t) = 0, \ t > 0 \quad (40)$$

$$v(0, y, t) = v(1, y, t) = v(x, 0, t) \\ = v(x, 1, t) = 0, \ t > 0 \quad (41)$$
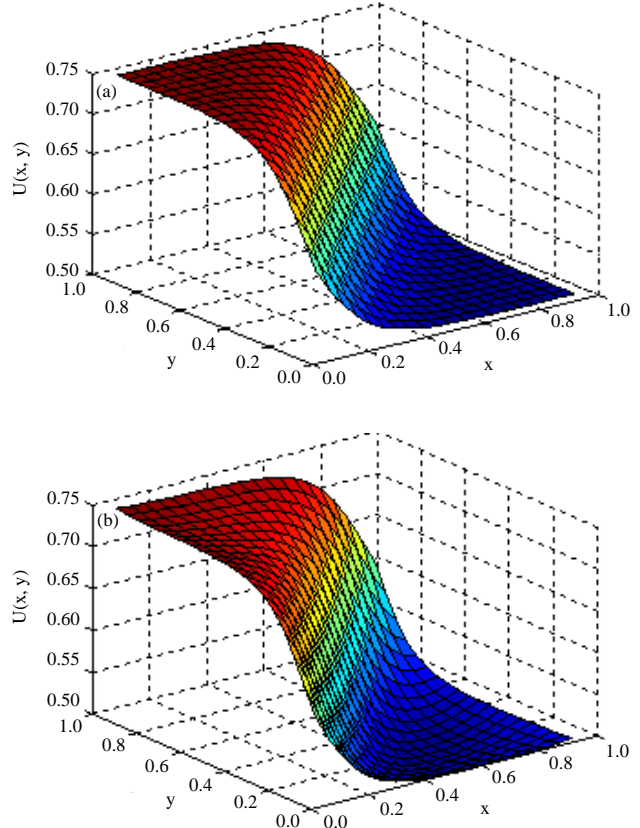
Fig. 3(a-b): Comparison of U-values for $(\varepsilon_{min}, \varepsilon_{max}) = (0.1, 10)$ at $t = 0.1$ with Re = 80 between the exact (left) and the computed ones (right)
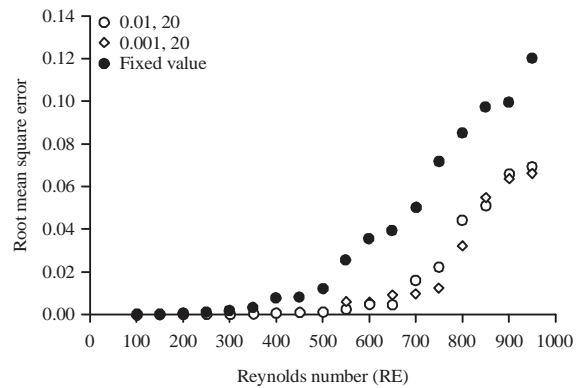
Fig. 4(a-b): Root mean square (RMS) error comparison at two intervals of $(\varepsilon_{min}, \varepsilon_{max})$ and that obtained using a fixed value of 3, computed with boundary nodes N = 120 and internal nodes L = 24 at t = 1.0

This leads to the exact solutions as the following forms:

$$u(x, y, t) = \frac{-4\pi \Upsilon \cos(2\pi x)\sin(\pi y)}{Re(2 + \Upsilon)\sin(2\pi x)\sin(\pi y))} \quad (42)$$

Table 10: Comparison of U-velocity for Re = 100, t = 0.5 with boundary nodes N = 80 and internal nodes L = 12, for (ε_{min}, ε_{max}) = (0.1, 1)

| | (ε_{min}, ε_{max}) = (0.1, 1) | | | |
Points	Exact	Numerical	Fixed ε = 1.5	Aminikhah[20]
(0.1, 0.1)	-0.011460121	-0.01251140	-0.00758995	-0.011463997
(0.5, 0.1)	0.015170656	0.01256220	0.00854112	0.015174171
(0.9, 0.1)	-0.013210753	-0.01399250	-0.00855622	-0.013198417
(0.3, 0.3)	0.009436724	0.00901225	0.00521580	0.009435086
(0.7, 0.3)	0.017548132	0.01452011	0.00745885	0.017771096
(0.1, 0.5)	-0.032300168	-0.03029582	-0.01225212	-0.032279521
(0.5, 0.5)	0.049093275	0.04526220	0.02115895	0.049013874
(0.3, 0.7)	0.009436724	0.01025885	0.00754821	0.009435086
(0.7, 0.7)	0.017548123	0.01650778	0.00899532	0.017771382
(0.1, 0.9)	-0.011460121	-0.01350025	-0.00895632	-0.011463997
(0.5, 0.9)	0.015170656	0.01325002	0.00458790	0.015174171
(0.9, 0.9)	-0.013210753	-0.01422152	-0.00744502	-0.013198421

Table 11: Comparison of V-values for Re = 100, t = 0.5 with boundary nodes N = 80 and internal nodes L = 12, for (ε_{min}, ε_{max}) = (0.1, 1)

| | (ε_{min}, ε_{max}) = (0.1, 1) | | | |
Points	Exact	Numerical	Fixed ε = 1.5	Aminikhah[20]
0.1, 0.1)	-0.01281279	-0.0170025	-0.0256622	-0.01281338
(0.5, 0.1)	0.00000000	0.0000012	0.0002150	-0.00000716
(0.9, 0.1)	0.01477007	0.0182212	0.0215002	0.01476979
(0.3, 0.3)	-0.01055058	-0.0122502	-0.0198852	-0.01054980
(0.7, 0.3)	0.01961941	0.0185592	0.0260210	0.01969169
(0.1, 0.5)	0.00000000	0.0000025	0.0013620	0.00000000
(0.5, 0.5)	0.00000000	0.0000001	0.0021104	0.00000000
(0.3, 0.7)	0.01055058	0.0089958	0.0155289	0.01054980
(0.7, 0.7)	-0.01961941	-0.0174125	-0.0321151	-0.01996921
(0.1, 0.9)	0.01281279	0.0145502	0.0142178	0.01281338
(0.5, 0.9)	0.00000000	0.0000003	0.0005210	0.00000716
(0.9, 0.9)	-0.01477007	-0.0160252	-0.0180215	-0.01476979

Fig. 5(a-b): Comparison of V-velocity for (ε_{min}, ε_{max}) = (0.1, 20) at t = 1 with Re = 1,000 between the exact (left) and the computed ones (right)

Table 12: Comparison of U-velocity for Re = 500, t = 0 with boundary nodes N = 80 and internal nodes L = 12, for (ε_{min}, ε_{max}) = (0.1, 1)

| | (ε_{min}, ε_{max}) = (0.1, 1) | | | |
Points	Exact	Numerical	Fixed ε = 1.5	Aminikhah[20]
(0.1, 0.1)	-0.0027524	-0.0025582	-0.0102596	-0.0027524
(0.5, 0.1)	0.0036962	0.0031558	0.0076215	0.0036962
(0.9, 0.1)	-0.0032733	-0.0045862	-0.0085510	-0.0032733
(0.3, 0.3)	0.0021888	0.0025505	0.0059025	0.0021888
(0.7, 0.3)	0.0047180	0.0048155	0.0081147	0.0047180
(0.1, 0.5)	-0.0075616	-0.0079932	-0.0094589	-0.0075616
(0.5, 0.5)	0.0119613	0.0111522	0.0310688	0.0119613
(0.3, 0.7)	0.0021888	0.0025201	0.0052585	0.0021888
(0.7, 0.7)	0.0047180	0.0046522	0.0085802	0.0047181
(0.1, 0.9)	-0.0027524	-0.0028582	-0.0078995	-0.0027522
(0.5, 0.9)	0.0036962	0.0032560	0.0108024	0.0036962
(0.9, 0.9)	-0.0032733	-0.0038475	-0.0087596	-0.0032733

Table 13: Comparison of V-velocity for Re = 500, t = 0.5 with boundary nodes N = 80 and internal nodes L = 12, for (ε_{min}, ε_{max}) = (0.1, 1)

| | (ε_{min}, ε_{max}) = (0.1, 1) | | | |
Points	Exact	Numerical	Fixed ε = 1.5	Aminikhah[20]
(0.1, 0.1)	-0.0030773	-0.0032295	-0.0048550	-0.0030773
(0.5, 0.1)	0.0000000	0.0002448	0.0015890	0.0000000
(0.9, 0.1)	0.0036596	0.0038201	0.0044225	0.0036596
(0.3, 0.3)	-0.0024472	-0.0025507	-0.0062256	-0.0024472
(0.7, 0.3)	0.0052749	0.0052798	0.0081258	0.0052749
(0.1, 0.5)	0.0000000	0.0001158	0.0072155	0.0000000
(0.5, 0.5)	0.0000000	0.0002052	0.0022598	0.0000000
(0.3, 0.7)	0.0024472	0.0022758	0.0101588	0.0024472
(0.7, 0.7)	-0.0052749	-0.0054471	-0.0091025	-0.0052750
(0.1, 0.9)	0.0030773	0.0035521	0.0075900	0.0030773
(0.5, 0.9)	0.0000000	0.0004122	0.0082145	0.0000000
(0.9, 0.9)	-0.0036596	-0.0035518	-0.0053489	-0.0036596

and:

$$v(x, y, t) = \frac{-2\pi\Upsilon\sin(2\pi x)\cos(\pi y)}{Re(2 + \Upsilon)\sin(2\pi x)\sin(\pi y)} \qquad (43)$$

where, Υ = exp (-5π^2 t/Re).

Table 10-13 provided results comparison amongst those produced in this study and both the exact solutions and other numerical investigation, Aminikhah[20]. The solution profiles obtained at high Reynolds number were shown in Fig. 5-6 where Fig. 7 provided the comparison of RMS at different values of both Reynolds numbers and ranges of (ε_{min}, ε_{max}).

Fig. 6(a-b): Comparison of U-velocity for $(\varepsilon_{min}, \varepsilon_{max}) = (0.1, 20)$ at t = 1 with Re = 1,000 between the exact (left) and the computed ones (right)

Fig. 7(a-b): Root mean square (RMS) error comparison at two intervals of $(\varepsilon_{min}, \varepsilon_{max})$ and that obtained using a fixed value of 1.5, computed with boundary nodes N = 120 and internal nodes L = 24 at t = 0.75

DISCUSSION

Regarding the use of inverse multiquadric (IMQ) type of radial basis functions (RBFs), it is not surprising to realize that only a few works available in literature. Most of these works, moreover, were carried out under the context of meshfree/meshless method. Some recent works that adopted this type of RBF are Chantawara[21] and Chuathong[22], where some fixed values of shape parameters were adopted. To validate results obtained in this paper, their suggested values of shape parameter were adopted.

The computational results produced in this work for the two benchmark examples are promising in several aspects. Firstly, by providing only two thresholds or bounding values of $(\varepsilon_{min}, \varepsilon_{max})$, searching for optimal choice becomes simpler. This feature can be seen more clearly when compared with those obtained by using a fixed value of ε, as shown in all Tables. The effect of the wide of the range $(\varepsilon_{min}, \varepsilon_{max})$ was seen not to have any significant effect on the final results quality ensuring the simplicity of the proposed shape form.

Another aspect that is desirable about the main findings of this study is the capability of the method to handle the instability of the problem when the Reynolds number increases. It is commonly found and is known to be a great challenge for any numerical procedure to tackle Burgers' equations at high Reynolds number ($\geq$500), the flow becomes more turbulent. One of our previous works and many other works, Keannakham *et al.*[12] and references herein, have shown that beyond this value of Reynolds number, the error norm is growing dramatically. It is shown clearly in this work that the proposed adaptive parameter is able to take into consideration the local physics that effects both the computing collocation matrix and the numerical algorithm itself.

CONCLUSION

In this study, the effectiveness of shape parameter contained in the inverse multiquadric type of RBF in conjunction with the method of DRBEM was investigated numerically. The investigation began with applying DRBEM to one of the most complicated PDEs namely Burgers' equations. Then a new form of shape parameter that behaves locally-adaptive, i.e., it varies accordingly to the local change of the physics of the problem which, here, is the local Reynolds number(Re) was proposed. The proposed variable shape form also contains both linear and exponential aspects based on the distance between the center node i and pointed node j in
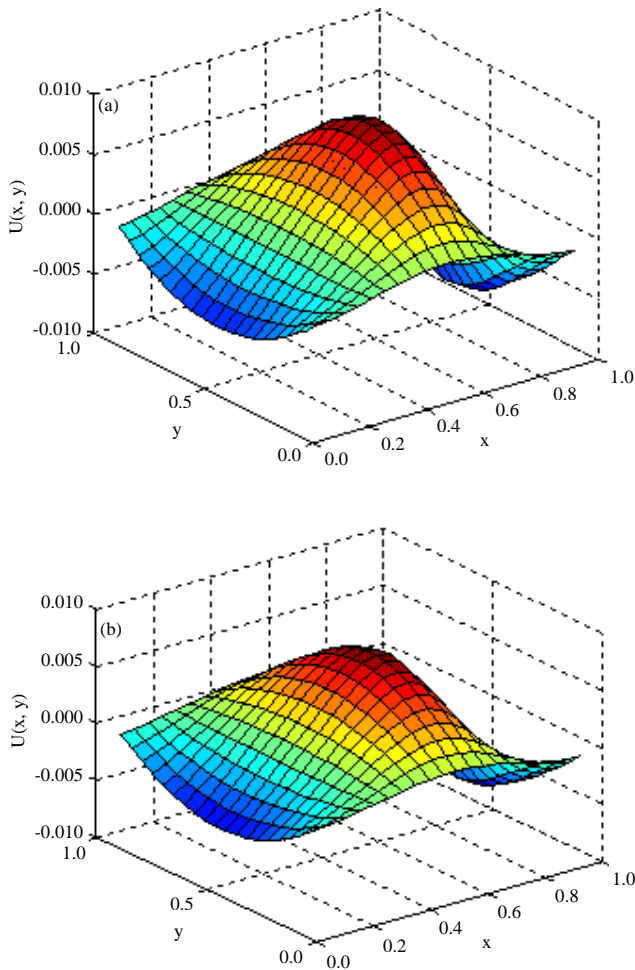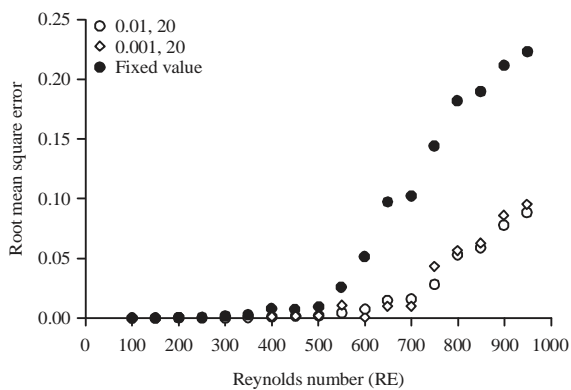
the RBF-collocation numerical method adopted. Some important conclusions can now be withdrawn from the investigation and they are as follows:

- DRBEM has successfully been applied to Burgers' equations using inverse multiquadric radial basis function at relatively high Reynolds number (Re)
- It is found from all the results obtained in this work that the proposed shape parameter can outperform the fixed ones and certainly deserves further investigation
- When compared with other numerical works, the accuracy lies in an acceptable level and moreover, gets better when the problem become advective dominated, at high Reynolds number

SIGNIFICANCE STATEMENT

This study discovers the benefit of using the local physical aspect of the problem as the indicator for the radial basis function's shape parameter which is designed to be locally adaptive. This study will help the researcher to uncover the critical area of choosing the optimal shape parameter when dealing with this particular form of equations. Thus, a new theory on these radial basis function's adaptive shape parameters and possibly other related fields, may be arrived at.

ACKNOWLEDGMENTS

REFFERENCES

1. Buhmann, M.D., 1990. Multivariate cardinal interpolation with radial-basis functions. Construct. Approximation, 6: 225-225.
2. Brebbia, C.A. and R. Butterfield, 1978. Formal equivalence of direct and indirect boundary element methods. Applied Math. Model., 2: 132-134.
3. Carlson, R.E. and T.A. Foley, 1991. The parameter R^2 in multiquadric interpolation. Comput. Math. Applic., 21: 29-42.
4. Hardy, R.L., 1971. Multiquadric equations of topography and other irregular surfaces. J. Geophys. Res., 76: 1905-1915.
5. Franke, C. and R. Schaback, 1998. Convergence order estimates of meshless collocation methods using radial basis functions. Adv. Comput. Math., 93: 381-392.
6. Zhang, X., K.Z. Song, M.W. Lu and X. Liu, 2000. Meshless methods based on collocation with radial basis functions. Comput. Mech., 26: 333-343.
7. Wang, J.G. and G.R. Liu, 2002. On the optimal shape parameters of radial basis functions used for 2-D meshless methods. Comput. Meth. Applied Mech. Eng., 191: 2611-2630.
8. Lee, C.K., X. Liu and S.C. Fan, 2003. Local multiquadric approximation for solving boundary value problems. Comput. Mech., 30: 396-409.
9. Burgers, J.M., 1948. A mathematical model illustrating the theory of turbulence. Adv. Applied Mech., 11: 171-199.
10. Nee, J. and J. Duan, 1998. Limit set of trajectories of the coupled viscous Burgers' equations. Applied Math. Lett., 11: 57-61.
11. Zhang, D.S., G.W. Wei, D.J. Kouri and D.K. Hoffman, 1997. Burgers' equation with high Reynolds number. Phys. Fluids, Vol. 9. 10.1063/1.869305
12. Keannakham, S., K. Chantawara and W. Toutip, 2014. [Optimal Radial Basis Function (RBF) for Dual Reciprocity Boundary Element Method (DRBEM) applied to coupled Burgers' equations with increasing Reynolds number]. Aust. J. Basic Applied Sci., 8: 462-476.
13. Toutip, W., 2001. The dual reciprocity boundary element method for linear and nonlinear problems. Ph.D. Thesis, University of Hertfordshire, Hertfordshire, United Kingdom.
14. Kansa, E.J., 1990. Multiquadrics: A scattered data approximation scheme with applications to computational fluid-dynamics-I surface approximations and partial derivative estimates. Comput. Math. Applied, 19: 127-145.
15. Kansa, E.J. and R.E. Carlson, 1992. Improved accuracy of multiquadric interpolation using variable shape parameters. Comput. Math. Applic., 24: 99-120.
16. Sarra, S.A., 2005. Adaptive radial basis function methods for time dependent partial differential equations. Applied Numer. Math., 54: 79-94.
17. Sarra, S.A. and D. Sturgill, 2009. A random variable shape parameter strategy for radial basis function approximation methods. Eng. Anal. Bound. Elements, 33: 1239-1245.
18. Fletcher, C.A., 1983. Generating exact solutions of the two dimensional Burgers' equations. Int. J. Numer. Meth. Fluids, 3: 213-216.
19. Biazar, J. and H. Aminikhah, 2009. Exact and numerical solutions for non-linear Burger's equation by VIM. Math. Comput. Model., 49: 1394-1400.
20. Aminikhah, H., 2012. A new efficient method for solving two-dimensional Burgers' equation. ISRN Comput. Math., 10.5402/2012/603280.
21. Chantawara, K., 2016. A numerical comparison of radial basis functions in applications of the dual reciprocity boundary element method to convection-diffusion problems. Ph.D. Thesis, Khon Kaen University, Thailand.
22. Chuathong, N., 2016. An automatic Centroid-Node Adaptive Meshless (CNAM) method for solving convection-diffusion problems. Ph.D. Thesis, Khon Kaen University, Thailand.